NASA MEMO 4-18-59A

NASA

MEMORANDUM

PREDICTED STATIC AEROELASTIC EFFECTS ON WINGS WITH SUPERSONIC LEADING EDGES AND STREAMWISE TIPS

By Stuart C. Brown

Ames Research Center
Moffett Field, Calif.

NATIONAL AERONAUTICS AND SPACE ADMINISTRATION
WASHINGTON
April 1959

NATIONAL AERONAUTICS AND SPACE ADMINISTRATION

MEMORANDUM 4-18-59A

PREDICTED STATIC AEROELASTIC EFFECTS ON WINGS WITH SUPERSONIC LEADING EDGES AND STREAMWISE TIPS

By Stuart C. Brown

SUMMARY

A method is presented for calculation of static aeroelastic effects on wings with supersonic leading edges and streamwise tips. Both chordwise and spanwise deflections are taken into account. Aerodynamic and structural forces are introduced in influence coefficient form; the former are developed from linearized supersonic wing theory and the latter are assumed to be known from load-deflection tests or theory.

The predicted effects of flexibility on lateral-control effectiveness, damping in roll, and lift-curve slope are shown for a low-aspect-ratio wing at Mach numbers of 1.25 and 2.60. The control effectiveness is shown for a trailing-edge aileron, a tip aileron, and a slot-deflector spoiler located along the 0.70 chord line. The calculations indicate that the tip aileron is particularly attractive from an aeroelastic standpoint, because the changes in effectiveness with dynamic pressure are small compared to the changes in effectiveness of the trailing-edge aileron and slot-deflector spoiler.

The effects of making several simplifying assumptions in the example calculations are shown. The use of a modified strip theory to determine the aerodynamic influence coefficients gave adequate results only for the high Mach number case. Elimination of chordwise bending in the structural influence coefficients exaggerated the aeroelastic effects on rolling-moment and lift coefficients for both Mach numbers.

INTRODUCTION

The characteristic low-aspect-ratio thin wings used for supersonic flight have aerodynamic and structural properties which differ considerably from the high-aspect-ratio subsonic wings for which methods for obtaining static aeroelastic effects, such as reference 1, have proved to be adequate. When thin wings are subjected to high dynamic pressure, there are large aeroelastic effects, which may include chordwise as well as spanwise deflections. Consequently, practical methods are needed to obtain supersonic aerodynamic influence coefficients and to calculate the resulting aeroelastic effects.

Several investigations of effects of chordwise deformations on aeroelastic effects at supersonic speeds have been made. One approach is to express the aerodynamic and structural characteristics in equation form, combine them, and then solve the combined equation for equilibrium conditions (e.g., refs. 2 and 3). However, the equations are only tractable for cases in which the structural and aerodynamic characteristics can be expressed in simplified form. An alternate approach, which is applicable to more general cases, is to obtain separate sets of structural and aerodynamic properties in the form of influence coefficients which define, respectively, the distribution of deflections and loads due to a load or deflection at specified points on a grid network. The resulting equations for static equilibrium are then solved numerically. Numerical methods have been developed for obtaining unsteady aerodynamic influence coefficients for use with flutter analysis (e.g., refs. 4 and 5). However, these methods which were derived for the more mathematically difficult problem of determining unsteady aerodynamic forces may be somewhat cumbersome when applied to the static case. Consequently, the aerodynamic influence coefficients which appear in this report should be useful for pseudostatic aeroelastic calculations which occur at frequencies where unsteady lift effects are small.

In the present report, a method, based on linearized potential flow theory, for the calculation of static aerodynamic influence coefficients is presented for wings with swept supersonic leading edges and streamwise tips. Both chordwise and spanwise distributions of loads and deflections are included. A numerical iteration method for combining the aerodynamic influence coefficients with a set of structural influence coefficients to calculate the resulting load distribution over a flexible wing is also given. The application of this method is illustrated by the calculation of the rolling performance of several types of lateral-control devices for a low-aspect-ratio thin wing with a supersonic leading edge at Mach numbers of 1.25 and 2.60.

SYMBOLS

$[A]$ aerodynamic influence coefficient matrix
(An element in the ith row and jth column indicates a load at station i due to an angle of attack at station j.)

$[B]$ matrix for converting to dimensionless load coefficients over a chordwise interval (eq. (9))

C_L lift coefficient, $\frac{\text{lift}}{qS}$

C_{L_α} rate of change of lift coefficient with angle of attack, per radian

C_l rolling-moment coefficient, $\frac{\text{rolling moment}}{qSb}$

C_{l_p} rate of change of rolling-moment coefficient with wing-tip helix angle, $\frac{pb}{2V}$

C_p pressure coefficient

[D] differentiating matrix used in converting to aerodynamic influence coefficients (eq. (11))

E modulus of elasticity, lb/sq ft

[F] structural influence coefficient matrix, streamwise angular deflection in radians at one station due to an applied load in pounds at another station
(An element in the ith row and jth column indicates the angle of attack at station i due to a load at station j.)

G dimensionless load coefficient from leading edge of panel to an arbitrary point, $\frac{\Gamma}{c_{av}U}$

ΔG dimensionless load coefficient over an arbitrary chordwise interval (eq. (9))

[I] spanwise integrating matrix for numerically integrating load coefficients

M Mach number

S total wing area including portion blanketed by fuselage, sq ft

S_p area of one exposed wing panel, sq ft

U free-stream velocity, ft/sec

b wing span, ft

c_{av} average chord based on total wing area, ft

c.p. chordwise center of pressure in local wing chords

k constant obtained from series used for calculating rolling-moment or lift coefficients for a flexible surface (eq. (20))

m cotangent of sweepback angle of leading edge of panel

p rolling velocity, radians/sec

q	dynamic pressure, lb/sq ft
t	maximum thickness, ft
x,y	longitudinal and lateral coordinates (fig. 1)
x_1,y_1	coordinates of apex of angle-of-attack panel (fig. 1)
x_t,y_t	coordinates of intersection of leading edge of panel and wing tip
α	angle of attack, radians
β	$\sqrt{M^2 - 1}$
Γ	circulation, sq ft/sec
δ	total aileron deflection, measured in a plane perpendicular to the y axis, radians
η	lateral coordinate in wing semispans
Λ	sweep angle, deg
ξ	longitudinal coordinate in average wing chords
τ	$\frac{\beta(y - y_1)}{x - x_1}$
τ_t	$\frac{\beta(y - y_t)}{x - x_t}$
$[\ ]$	rectangular matrix
$\{\ \}$	column matrix
$\lfloor\ \rfloor$	row matrix
$\lfloor 1 \rfloor$	row matrix in which all elements are unity

Subscripts

A	antisymmetric
E	incremental value due to flexibility
F	flexible case equilibrium value
R	rigid case value

S	symmetric
le	leading edge
te	trailing edge
tip	tip aileron

ANALYSIS

This section is concerned with the method of determining the resultant aerodynamic force on a flexible wing with supersonic leading and trailing edges and streamwise tips due to such initial angle-of-attack distributions as deflected ailerons and rolling velocities. First, the manner of obtaining a set of aerodynamic influence coefficients (defined as the loading coefficient at one station due to a unit angle of attack at another station) is given. From these coefficients, the aerodynamic loading and the resultant aerodynamic force due to an arbitrary distribution of angle of attack in both the spanwise and chordwise directions may be obtained. Then, a set of structural influence coefficients, which will be assumed already available in the form of an angle of attack at one station due to a load at another station, will be combined with the aerodynamic influence coefficients to determine an equilibrium angle-of-attack distribution and resulting aerodynamic force.

Aerodynamic Influence Coefficients

The calculation of the aerodynamic influence coefficients is based on linearized potential flow theory. First, the equations are determined for the aerodynamic load coefficients at various regions of the wing due to a part of the wing, or panel, deflected at 1-radian angle of attack (fig. 1). The panel has a supersonic leading edge which extends outboard at slope m from an apex at an arbitrary point x_1,y_1 to the wing tip. Networks of control points which correspond to load coefficient locations and to locations of apexes of the deflected panels are selected and a set of load coefficients for each panel location is calculated. These load coefficients are then converted to aerodynamic influence coefficient form by suitable superposition of the panels. This superposition is determined by the coefficients required to numerically differentiate an arbitrary angle-of-attack distribution.

The equations used for obtaining the load coefficients in the various regions indicated in figure 1 due to a panel at a unit angle of attack are summarized here, while a more detailed presentation is given in appendix A. The equations are first presented in the form of load coefficients which are proportional to the streamwise integration of pressures from the

leading edge of the panel to the desired load point, x,y. While somewhat simpler equations could have been written in terms of pressure coefficients, a brief numerical analysis indicated that a considerably larger number of stations would then have to be used to obtain a given accuracy. This was particularly true for cases with even moderately swept leading edges.

The load coefficients for points x,y, which are located in regions affected only by the inboard portion of a panel at a unit angle of attack whose apex is at x_1,y_1, can be expressed by the following equations:

Region I ($\tau < -1$)

$$G = 0 \tag{1}$$

Region II ($-1 \leq \tau \leq 1$)

$$G = \frac{2(x - x_1)}{\pi\beta c_{av}} \left[\frac{\beta m - \tau}{\sqrt{\beta^2 m^2 - 1}} \cos^{-1}\left(\frac{1 - \beta m\tau}{\beta m - \tau} \right) + \tau \cosh^{-1}\left| \frac{1}{\tau} \right| \right] \tag{2}$$

where $0 \leq \cos^{-1}( ) \leq \pi$.

Region III ($\tau > 1$)

$$G = \frac{2(x - x_1)(\beta m - \tau)}{\beta c_{av}\sqrt{\beta^2 m^2 - 1}} \tag{3}$$

These equations are valid for the three regions isolated from the wing tip ($\tau_t < -1$) and may be used to calculate loading coefficients for arbitrary angle-of-attack distributions for plan forms whose edges are all supersonic.

For the remaining regions indicated by figure 1, the loss in loading due to the side edge must be taken into account. The following equation, expressed in terms of the distance from the tip of the leading edge of the panel x_t,y_t, represents the loss in loading coefficients for

Regions IV and V ($-1 \leq \tau_t \leq 0$)

$$G = \frac{2(x - x_1)}{\pi\beta c_{av}\sqrt{\beta^2 m^2 - 1}} \left\{ -(\beta m - \tau_t)\cos^{-1}\left[\frac{\beta m + \tau_t(2\beta m + 1)}{\tau_t - \beta m} \right] + 2\sqrt{\beta m(-\tau_t)(1 + \tau_t)(\beta m + 1)} \right\} \tag{4}$$

For region VI, which is defined by the equation

$$x - x_1 > \beta(2y_t - y_1 - y) \tag{5}$$

a separate load coefficient equation is used. For this region, it is convenient to combine the equation for the loading due to the inboard portion of the panel with the equation for the tip effect to give

$$G = \frac{2(y_t - y_1)}{\pi c_{av}} \left[\left(\frac{y - y_1}{y_t - y_1} \right) \cosh^{-1} \left| \frac{2(y_t - y_1)}{y - y_1} - 1 \right| + 2\sqrt{1 - \frac{y - y_1}{y_t - y_1}} \right] \quad (6)$$

The equations that give the load coefficients for a point x,y, which may be located in various regions with respect to a panel at a unit angle of attack with an apex at x_1,y_1, are summarized in figure 1.

The load coefficient due to a panel at a unit angle of attack on the right-hand side of the wing center line can be calculated from the previous equations for all points on both sides of the wing center line which are not affected by the wing tip on the opposite side from the deflected panel. For points which are affected by the opposite wing tip, an additional correction would be required. However, for cases where this additional tip effect occurs only for points near the tip of the opposite side of the wing from the deflected panel, the loss in loading will be small and can often be neglected, and hence, equation (2) can still be used to obtain the load coefficient. The equation for this region is included in appendix A in order to determine limiting cases, however.

From the calculated load coefficients for all load stations on the wing which result from a set of panel stations on one side, the matrix for the antisymmetric load coefficients $[G_A]$ and the matrix of symmetric load coefficients $[G_S]$ can be formed as follows:

$$[G_A] = [G(x,y,x_1,y_1)] - [G(x,-y,x_1,y_1)] \quad (7)$$

$$[G_S] = [G(x,y,x_1,y_1)] + [G(x,-y,x_1,y_1)] \quad (8)$$

These load coefficients represent loads resulting from the integration of pressures from the leading edge of a panel to a given load point, x,y.

In order to obtain a chordwise distribution of load coefficient that can be used in conjunction with the structural influence coefficients, the operation

$$\Delta G = \frac{\partial G}{\partial \xi} d\xi$$

is performed for each chordwise interval by subtracting the value of load coefficient at the back of each interval from the value at the front of the interval. If desired, the differentiation could be calculated more accurately through use of polynomial curve fitting (e.g., ref. 12). Note that while the reduction of the G load coefficients to a chordwise incremental form, ΔG, corresponds to expressing them as

average pressures over the interval, a smoothing effect has been introduced to make the subsequent numerical integration more accurate than if pressure coefficients had been used. The operation may be expressed symbolically by a matrix [B] as

$$[\Delta G] = [B][G] \tag{9}$$

Each column of the matrix [ΔG] represents the distributed loading resulting from a panel such as an aileron at a unit angle of attack. The load coefficients for control surfaces which do not coincide with the panel control points can be determined by interpolation of the panel values since the variations in these values are generally quite smooth.

The ΔG panel load coefficients will now be adapted to the determination of the loading due to a continuous arbitrary angle-of-attack distribution. The following equation, in which the dimensionless variables ξ,η are used in place of x,y, will be evaluated numerically for the case of zero angle of attack at the plane of symmetry.

$$\Delta G^*(\xi,\eta) = \int_0^1 \int_{le}^{te} \Delta G(\xi,\eta,\xi_1,\eta_1) \frac{\partial}{\partial \eta_1} \left[\alpha_{le}(\eta_1) + \frac{\partial \alpha(\xi_1,\eta_1)}{\partial \xi_1} \right] d\xi_1 d\eta_1 \tag{10}$$

where $\Delta G^*(\xi,\eta)$ is the load coefficient distribution resulting from an arbitrary angle-of-attack distribution, $\alpha(\xi_1,\eta_1)$. In order for the $\Delta G(\xi,\eta,\xi_1,\eta_1)$ function in integral form to correspond to the previously given ΔG in matrix form, a chordwise interval in ξ would have to be specified. This need not be done explicitly, however, since the equation is used only to illustrate the operations performed by the matrices.

In evaluating equation (10) numerically, it will be convenient to define a quantity representing the product of the following terms and operations.

$$A(\xi,\eta,\xi_1,\eta_1) = \Delta G(\xi,\eta,\xi_1,\eta_1) \frac{\partial}{\partial \eta_1} \left[(\ )_{le} + \frac{\partial (\ )}{\partial \xi_1} \right] d\xi_1 d\eta_1$$

This quantity A, when expressed in terms of discrete intervals of the coordinates, is in the form of a load coefficient at one station due to a unit angle of attack at another station and will be called the aerodynamic influence coefficient matrix.

$$[A] = [\Delta G][D] \tag{11}$$

The load coefficient due to an arbitrary angle-of-attack distribution can then be evaluated by use of a single matrix multiplication.

$$\{\Delta G^*\} = [A]\{\alpha\}$$

The matrix [D] performs the operation $\frac{\partial}{\partial \eta_1}\left[\left(\ \right)_{le} + \frac{\partial(\ )}{\partial \xi_1}\right]$ by numerical differentiation and multiplies by the corresponding integration intervals $d\xi_1 d\eta_1$. The numerical differentiation coefficients used in this matrix are based on coefficients obtained by polynomial curve fitting (e.g., ref. 12) of the angle-of-attack curves. The degree of the polynomial employed depends upon the shape of the angle-of-attack curves and the accuracy desired. Each row of the matrix [D] represents the product of the integration interval and the coefficients which determine the rate of change of angle of attack that results from an arbitrary angle-of-attack distribution. Each column represents the product of the integration interval and the coefficients of the slopes at the neighboring stations which produce a unit angle of attack at one station and zero angle of attack at the remaining stations. Thus, the aerodynamic influence coefficient matrix [A] represents the loading which results from a superposition of panels that give a unit angle of attack at one station and zero angle of attack at the remaining stations.

A program for calculating the aerodynamic influence coefficients was set up for an IBM 650 digital computing machine.

Structural Influence Coefficients

For the analysis of this report, the structural influence coefficient matrix [F] will be assumed available from either experiment or theory in the form of a change in angle of attack at one station due to a concentrated load at another station. Where possible, of course, it is desirable to measure the coefficients directly from the actual structure. While a number of prediction methods are available (e.g., refs. 6 through 10), the accuracy depends upon the complexity of the structure and the plan form. Although prediction methods which will yield angle-of-attack distributions due to applied loads are adequate for higher aspect ratios, they may not be adequate for low-aspect-ratio wings where chordwise bending and root conditions become of greater importance.

Calculation of the Stability Derivatives for a Flexible Wing

In order to determine a particular stability derivative, the sets of aerodynamic and structural influence coefficients which were obtained for corresponding points on a plan form must be combined, and the equilibrium angles of attack and the resulting forces and moments on the flexible wing must be calculated. The equation for the incremental angle of attack due to flexibility, α_E, which results from an initial arbitrary distribution of angle of attack for the undeflected or rigid wing, α_R, may be expressed in integral equation form as

$$\alpha_E(\xi_1,\eta_1) = qS\int_0^1\int_{le}^{te}\left\{[F(\xi_1,\eta_1,\xi,\eta)]\int_0^1\int_{le}^{te}\frac{\partial G(\xi,\eta,\xi_1,\eta_1)}{\partial\xi}\frac{\partial}{\partial\eta_1}\left[\alpha_{F_{le}}(\eta_1)+\frac{\partial\alpha_F(\xi_1,\eta_1)}{\partial\xi_1}\right]d\xi_1 d\eta_1\right\}d\xi\,d\eta \quad (12)$$

where $\alpha_F = \alpha_R + \alpha_E$.

When the previously discussed aerodynamic and structural influence coefficients are used, and a spanwise integrating matrix [I] is introduced for numerically integrating the load coefficients in the final integration, equation (12) can be expressed in matrix form as

$$\{\alpha_E\} = qS[F][I][A_A]\{\alpha_R + \alpha_E\} \quad (13)$$

The relaxation process described in reference 11, in which the incremental angle of attack $\{\alpha_E\}$ is expressed in series form, is used to evaluate this equation. Once the incremental angle-of-attack distribution is obtained, the resulting lift and moment coefficients due to the rigid and incremental angles of attack can then be expressed in an analogous series form. The antisymmetric case will be considered first. The rolling-moment coefficient due to a rigid angle-of-attack distribution is given by the equation

$$C_{l_R} = [\eta][I][A_A]\{\alpha_R\} \quad (14)$$

Since the incremental angle-of-attack distribution due to flexibility is small in comparison with the rigid value, a first approximation to the incremental angle of attack $\{\alpha_E\}$ is obtained through use of equation (13)

$$\left\{\frac{\alpha_1}{q}\right\} = S[F][I][A_A]\{\alpha_R\} \quad (15)$$

For convenience, the incremental rolling-moment coefficient is defined in terms of a unit value of dynamic pressure.

$$C_{l_1} = [\eta][I][A_A]\left\{\frac{\alpha_1}{q}\right\} \quad (16)$$

The loading represented by C_{l_1} causes an additional increment in the angle of attack due to flexibility which is determined by

$$\left\{\frac{\alpha_2}{q^2}\right\} = S[F][I][A_A\left\{\frac{\alpha_1}{q}\right\} \quad (17)$$

and

$$C_{l_2} = [\eta][I][A_A]\left\{\frac{\alpha_2}{q^2}\right\} \quad (18)$$

The procedure is repeated so that the rolling-moment coefficient for the flexible case can then be expressed in series form as

$$C_{l_F} = C_{l_R} + C_{l_1}q + C_{l_2}q^2 + C_{l_3}q^3 + \cdots \tag{19}$$

After the relaxation process is repeated a sufficient number of times, the ratio of succeeding coefficients, $C_{l_n}/C_{l_{n-1}}$, approaches a constant, $-k$. The effect of succeeding terms can then be expressed in analytical form as $C_{l_n}q/(1+kq)$. For instance, if the value of C_{l_4}/C_{l_3} and the succeeding ratios is a constant, the equation for rolling-moment coefficient can be expressed as

$$C_{l_F} = C_{l_R}\left\{1 + \frac{C_{l_1}}{C_{l_R}}q\left[1 + \frac{C_{l_2}}{C_{l_1}}q\left(1 + \frac{C_{l_3}q/C_{l_2}}{1+kq}\right)\right]\right\} \tag{20}$$

An analogous expression for lift coefficient can be obtained in a similar manner through use of the symmetric aerodynamic influence coefficients and the following equation.

$$C_L = [1][I][A_S]\{\alpha\} \tag{21}$$

The value of $q = -1/k$ is the dominant characteristic or eigenvalue of dynamic pressure of the system of simultaneous equations (eq. 13). For an unswept or sweptforward wing, $1/k$ is usually negative and represents the dynamic pressure for which divergence occurs. For a sweptback wing, $1/k$ is usually positive, and hence no real divergence speed is encountered.

NUMERICAL EXAMPLE

Description of Example

Geometry.- The preceding analysis has been applied to the hypothetical supersonic configuration shown in figure 2. Pertinent geometric characteristics are shown in the figure. Since wing flexibility may have a major effect on lateral control, the following controls were investigated: a 0.143-semispan full-chord tip aileron, a 0.429-semispan 1/3-chord trailing-edge aileron, and a slot-deflector spoiler with a chordwise center of pressure assumed to be acting along the 70-percent chord line and extending from 0.500 semispan to 0.857 semispan.

Aerodynamic influence coefficients.- Aerodynamic influence coefficients were calculated for two Mach numbers, 1.25 and 2.60, which are about the limits for which the lifting-surface theory should be useful for this plan form. The lower Mach number, for which the Mach wave sweep angle is 36.8° and the leading edge is only slightly supersonic, represents

a condition of large tip effect and interactions among the deflected surfaces. The higher Mach number, with a Mach wave sweep angle of 67.4°, represents a condition of only small interaction effects.

While a more complete analysis would have included an approximation of the effects of wing-body interference, these effects were neglected in this case since the principal emphasis was on lateral derivatives for which wing-body interference is small. The wing-body combination was replaced by a wing alone extending over the wing area blanketed by the fuselage. The only portion considered flexible was the part outboard of the wing-body juncture. However, the aerodynamic interaction effects between the flexible and rigid portions of the surfaces were still included.

The exposed plan form was divided into a grid of 15 sections with 5 equidistant spanwise intervals and 3 equidistant chordwise intervals (fig. 2). Since the aerodynamic loading varies considerably near the tip but is zero at the tip, the farthest outboard load station was a half interval from the tip. In addition, two spanwise intervals were used for the portion of the wing blanketed by the fuselage. After the coordinates for the grid were selected, the load coefficients $[G_A]$ and $[G_S]$ were calculated from equations (1) through (8) for both load and deflection locations. The matrix [B] for converting the [G] coefficients to the increment in load coefficient acting over each interval between adjacent chordwise grid points, and the matrix [D] for differentiating the angle-of-attack distribution are given in tables II and III, respectively. In determining the matrix [D], the numerical differentiation was calculated in the streamwise and constant percent chord directions since the wing stations for the influence coefficients were arranged in these directions. An examination of the structural influence coefficients showed that the variations in angle of attack in the chordwise direction were less than those in the spanwise direction. Hence, a linear curve fit of two neighboring points was used to obtain coefficients for angle-of-attack slopes in the chordwise direction, while in the spanwise direction, coefficients for slopes based on a parabolic curve fit of three neighboring points (e.g., ref. 12) were used. Since only two neighboring points were used to determine the slopes in the chordwise direction, the midpoints of the intervals were selected as reference locations for the slopes. A more detailed description is given in appendix B. The aerodynamic influence coefficients were then calculated from equations (9) and (11).

Structural influence coefficients.- The structural influence coefficients, table I, were estimated from available measured influence coefficients of thin structures with somewhat similar plan forms. They are listed in a dimensionless form that is based on the deflection equation from plate theory which is applicable to the relatively thin wings considered. These coefficients represent typical variations in deflections of a homogeneous structure wing with the maximum thickness near the midchord. The addition of lateral controls to the structure was assumed

to be such that the structural influence coefficients were unchanged. The coordinates for the 15 deflection stations were located at 5 equally spaced intervals from the wing-body juncture to the wing tip and at the midpoints of 3 equal intervals in the chordwise direction (fig. 2).

Calculation of the stability derivatives.- The rolling effectiveness of the trailing-edge aileron, tip aileron, and spoiler, and the damping in roll (C_{l_p}), as well as the lift effectiveness (C_{L_α}), were evaluated for a range of dynamic pressures for both Mach numbers through use of equations (13) through (21). The determination of the spanwise integrating matrix [I] which appears in these equations is described in appendix B and listed in table IV. Calculations were also made using simplifications of the aerodynamic and structural characteristics described in the next section.

In general, the convergence of the iteration process described in the analysis section was good in the calculation of results from this example. For the high Mach number, only two iterations of the rolling-moment or lift coefficient ratios described in the analysis section were needed to define the curves over the range of dynamic pressures shown. This was the same number required for the high-aspect-ratio configuration described in reference 1. For the low Mach number, the number of iterations required depended upon the rigid-wing load distribution. For the trailing-edge aileron, only two iterations were required, while for the other quantities, additional iterations were needed up to a maximum of five for C_{l_p} when the complete aerodynamic and structural influence coefficients were used. For all cases, the eigenvalue for the symmetric loading was essentially the same as that for the antisymmetric loading.

Results and Discussion

The calculations made of the lateral-control effectiveness and the stability derivatives C_{l_p} and C_{L_α} over a range of dimensionless dynamic pressures for Mach numbers of 1.25 and 2.60 are discussed and comparisons are made of the results by the complete method with those obtained by several aerodynamic and structural simplifications.

Complete method results.- The ratios of stability derivatives for the flexible and rigid wings are shown in figure 3. The rigid values are listed in the following table to provide an additional comparison:

M	C_{L_α}	C_{l_p}	$C_{l_{\delta_{te}}}$	$C_{l_{\delta_{tip}}}$
1.25	4.51	0.405	0.0981	0.0411
2.60	1.62	.197	.0334	.0247

The rigid values shown in the table were obtained by the numerical integration and were in good agreement with corresponding analytical values.

This comparison indicates that the number of spanwise stations selected was adequate for this example. Since the chordwise locations of centers of pressure have considerable influence on the aeroelastic effects, the centers of pressure of the rigid-wing loadings are also shown (fig. 4). The centers of pressure near the tip are of greatest interest since the largest structural deflections occur in this region.

Looking first at the curves in figure 3 for the Mach number of 1.25, the variations of flexible-rigid ratios with dynamic pressure are considerably different for the various derivatives. The trailing-edge aileron, with a rigid-wing center of pressure at the 0.83 chord, has the greatest loss with dynamic pressure. The loss for the spoilers, with a center of pressure at 0.70 chord, is considerably less, and the dynamic pressure for which control reversal occurs is approximately double that of the trailing-edge aileron. The quantities whose centers of pressure for the rigid case are farthest forward (fig. 4), C_{L_α}, tip aileron C_{l_δ}, and C_{l_p} decrease only slightly or even increase in effectiveness. An examination of the structural influence coefficients shows that the average rotation about an axis perpendicular to the plane of symmetry at each spanwise station may be represented approximately by an elastic axis from about 0.30 chord near the tip to about 0.50 chord toward the root. The changes in rolling-moment coefficient due to flexibility are greatest when the differences between the approximate elastic axis location and the centers of pressure of the rigid loadings are the largest.

The increase in C_{l_p} with dynamic pressure shown in figure 3(a) could be quite detrimental to the rolling performance of configurations with rolling-control effectiveness that decreases with dynamic pressure. The factors that contribute to this variation in C_{l_p} can be explained if they are examined in a manner similar to the series development used in the calculations. Since the center of pressure of the rigid C_{l_p} loading is fairly close to the approximate elastic axis, the average incremental angle of attack due to this loading is quite small. However, a significant amount of chordwise bending is present and the center of pressure of the incremental load due to this bending is near the 0.70 chord because of the relatively flexible afterportion of the wing. This increment in angle of attack represents practically the total deflection mode shape at very low dynamic pressures, and the resulting increment of loading will tend to decrease the magnitude of the rolling moment. The mode shape at higher dynamic pressures can be visualized if the total wing distortion is separated into (1) this initial mode shape, for which only the magnitude will vary with dynamic pressure and which will produce a rolling-moment increment of opposite sign from the rigid value, and (2) the additional deflections due to loads and deflections that result from the initial mode shape and which produce a rolling-moment increment of the same sign as the rigid value. Since the center of pressure of the initial mode shape is approximately the same as that of the spoiler, the additional deflections will yield an incremental rolling moment which is of equal but opposite magnitude to that due to the initial mode shape at a dynamic pressure approximately the same as that for which rolling-moment

reversal occurs for the spoiler. Therefore, the C_{l_p} rolling-moment ratio will increase to unity at this dynamic pressure. At higher values of dynamic pressure, the rolling-moment ratio for C_{l_p} will be greater than unity.

At the higher Mach number, changes with dynamic pressure would be expected to be similar but less because of the reduction in two-dimensional lift-curve slope. This trend is shown by the trailing-edge aileron and spoiler curves whose rigid-wing centers of pressure are the same for both Mach numbers. However, the values of C_{L_α}, C_{l_p}, and tip aileron C_{l_δ}, all decrease with dynamic pressure because the centers of pressure of the rigid loadings are farther aft than for the low Mach number.

Aerodynamic simplifications.- In order to determine under what conditions simplifications of the lifting-surface theory could be made, the following two simplifications were investigated. One simplification used was to assume that the magnitude of the load at each station depended only on the local angle of attack and was equal to the loading obtained at that station if the entire wing was at the same angle of attack. Thus the aerodynamic influence coefficient matrix was a diagonal matrix with values equal to those for the wing at a unit angle of attack. The results obtained from these values will be referred to as modified strip theory results. An additional simplification of the modified theory was made by letting the three aerodynamic coefficients at each spanwise station be of equal value, but leaving their sum the same as in the previous case. Thus, the chordwise distribution of loading would be proportional to the local angle of attack, which is analogous to the two-dimensional case. Results obtained from this additional modification will be referred to as simplified strip theory results.

Comparisons of the flexible-rigid ratios from the modified strip theories with those from the complete aerodynamic theory are shown in figure 5. At the lower Mach number, the values of rolling-moment and lift coefficient ratios from the strip theories are seen to be much less than those from the lifting-surface theory. This discrepancy is particularly true for the simplified strip theory case which underestimates the values of C_{l_p} by approximately 50 percent at the higher dynamic pressures. As mentioned previously, the effect of the tip as predicted by lifting-surface theory is to reduce the loading near the tip, with the greatest reductions occurring over the afterportions. Hence, if a strip theory based on a constant angle-of-attack distribution is used, the results will underestimate tip effects due to wing distortions since these angle-of-attack distributions are concentrated more toward the tip. Thus the incremental rolling moments due to flexibility predicted by the strip theories will tend to be larger so that the resultant rolling-moment ratio will decrease more with dynamic pressure. Another reason for the deviations in C_{l_p} is that the chordwise center of pressure of the rigid loading from the strip theories is farther aft than that from lifting-surface theory and therefore it is farther from the approximate elastic axis.

The modified strip theory results for C_{L_α} show good agreement with the lifting-surface theory even for the lower Mach number, since the rigid-wing loadings are the same for the two theories and the variation of $C_{L_{\alpha_F}}/C_{L_{\alpha_R}}$ with dynamic pressure is small for this rigid-wing center-of-pressure location as it is close to the approximate elastic axis. However, the center of pressure of the rigid C_{L_α} loading predicted by the simplified strip theory is a little farther aft than that predicted by lifting-surface theory; therefore, a slightly greater reduction of $C_{L_{\alpha_F}}/C_{L_{\alpha_R}}$ with dynamic pressure occurs. For the trailing-edge aileron, predictions of reversal dynamic pressure obtained by use of the modified strip theories are about 25 percent lower than those predicted when lifting-surface theory is used.

At the higher Mach number, good agreement is obtained between the strip theory and lifting-surface theory results because the tip and other aerodynamic interaction effects extend over only small spanwise portions of the wing.

Structural simplifications.- To get an indication of the importance of chordwise bending for this case, a simplification of the structural matrix was made by assuming that each spanwise section rotated in the streamwise direction as a unit. Then, each load was assumed to produce an angle of attack at a spanwise station equal in magnitude to the average of the values of the deflections at the three chordwise stations.

Comparisons of the flexible-rigid ratios with and without chordwise bending are shown in figure 6. At both Mach numbers, neglecting chordwise bending makes an appreciable difference in the aeroelastic effects. The aileron reversal dynamic pressure is underestimated by about 15 percent while decreases in C_{l_p} and C_{L_α} also occur in both cases. The reason for this trend can be explained as follows: An examination of the structural influence coefficients (table I) indicates that the structure is relatively flexible over the afterportion of the wing in that deviations from the average deflection tend to be greater in the afterregions and also loads applied to the afterportions produce greater deflections. At low dynamic pressures, the average value of incremental angle of attack due to deflections will be the same for the two cases with and without chordwise bending, but the angle of attack will be concentrated farther aft for the chordwise bending case. These angles of attack will produce approximately the same increment of rolling-moment coefficient which will tend to counteract the originally applied load. However, as dynamic pressure is increased, these incremental loads will produce an additional angle-of-attack change. For the case where chordwise bending is neglected, the latter angle-of-attack increment will be smaller than the complete structure case since the loads are smaller over the afterportion of the wing. Consequently, the loading resulting from the latter angle of attack, which is in the direction of the originally applied loading, is smaller than the complete structure case. Thus the rolling-moment coefficient ratio will decrease more at the high dynamic

pressures when chordwise bending is neglected. The lifting-surface effects of Mach number are relatively small in this comparison since, as may be determined from figure 6, the values of the flexible-rigid ratios for the cases with and without chordwise bending are approximately the same for equal values of the parameter q/β. This parameter takes into account the differences in two-dimensional lift-curve slopes for the two Mach numbers.

It is of interest to note that, when chordwise bending is included, the magnitude of the constant k is greater since the corresponding chordwise angle-of-attack distribution and load distribution are farther aft and hence a larger deflection and load occurs. Thus the resulting contribution of the chordwise bending in this case is to reduce the possibility of a divergent condition. For a case with the largest deflections toward the forward part of the wing, a trend toward divergence would be expected.

CONCLUDING REMARKS

A method has been presented for calculating lifting-surface aerodynamic influence coefficients for swept wings with supersonic leading edges. Through use of these aerodynamic influence coefficients, together with a set of structural influence coefficients, aeroelastic effects were calculated for an example low-aspect-ratio wing for Mach numbers of 1.25 and 2.60. An evaluation of results from these example calculations for several lateral controls and stability derivatives has led to the following conclusions:

1. Comparisons of results from a modified strip theory with those from the lifting-surface theory indicate that the modified strip theory was satisfactory for the high Mach number case, but inadequate for the low Mach number case. A large part of the discrepancy was due to the fact that the modified strip theory did not predict with sufficient accuracy the chordwise distribution of loading near the tip which resulted from the wing deflections.

2. For this example, neglecting chordwise bending tended to predict greater reductions in rolling-moment and lift coefficients with dynamic pressure than when the complete structural characteristics were used.

3. The trailing-edge aileron had the greatest loss in effectiveness of all the controls studied and resulted in a relatively low reversal speed. The loss in lateral-control effectiveness of a slot-deflector spoiler was considerably less, having a reversal dynamic pressure

approximately double that of the trailing-edge aileron. The tip aileron had the least variation in control effectiveness with dynamic pressure, and at the lower Mach number the effectiveness actually increased at high dynamic pressures.

Ames Research Center
National Aeronautics and Space Administration
Moffett Field, Calif., Jan. 21, 1959

APPENDIX A

DERIVATION OF EQUATIONS FOR AERODYNAMIC LOADING

The equations for the loading due to the wing panel at 1-radian angle of attack shown in figure 1 will be developed. This development is equivalent to the determination of the loading due to an aileron deflection for various regions over a wing including the regions of interaction effects between the inboard end of the aileron and the tip. Linearized potential flow theory is used. While, of course, part of this development has been given in the literature previously, the derivation of all the equations is indicated for completeness. In determining the resulting loads due to an arbitrary angle-of-attack distribution, it was found desirable to express the aerodynamic coefficients in terms of circulation coefficients rather than pressure coefficients, since the total load could then be obtained with greater accuracy provided a sufficient number of control points were used to define the angle-of-attack distribution. This was particularly true for cases with swept leading edges.

The equations for the pressure on the top surface for the inboard portion of a panel at 1-radian angle of attack were given in reference 13 and are expressed by the notation shown in figure 1 as

$$\beta C_p = 0 \qquad (\tau < -1) \tag{A1}$$

$$\beta C_p = \frac{2\beta m}{\pi\sqrt{\beta^2 m^2 - 1}} \cos^{-1} \frac{1 - \beta m \tau}{\beta m - \tau} \qquad (-1 \leq \tau \leq 1) \tag{A2}$$

where $0 \leq \cos^{-1}\left(\frac{1 - \beta m \tau}{\beta m - \tau}\right) \leq \pi$.

$$\beta C_p = \frac{2\beta m}{\sqrt{\beta^2 m^2 - 1}} \qquad (\tau > 1) \tag{A3}$$

The last equation represents the pressure over the portion of the panel which is undisturbed by either edge.

To get the dimensionless load coefficient $G = \Gamma/Uc_{av}$ between the leading edge of the panel and a point $(x - x_1)$, the following equation was used to integrate the previous equations in the streamwise direction.

$$G = \frac{1}{c_{av}} \int_{(x - x_1)_{le}}^{x - x_1} C_p d(x - x_1) \tag{A4}$$

The equations for the load coefficient become

$$G = 0 \qquad (\tau < -1) \tag{A5}$$

$$G = \frac{2(x - x_1)}{\pi\beta c_{av}} \left(\frac{\beta m - \tau}{\sqrt{\beta^2 m^2 - 1}} \cos^{-1} \frac{1 - \beta m \tau}{\beta m - \tau} + \tau \cosh^{-1} \left| \frac{1}{\tau} \right| \right) \qquad (-1 \leq \tau \leq 1) \tag{A6}$$

$$G = \frac{2(x - x_1)(\beta m - \tau)}{\beta c_{av} \sqrt{\beta^2 m^2 - 1}} \qquad (\tau > 1) \tag{A7}$$

Equations (A5), (A6), and (A7) can be used to calculate the load coefficient distribution due to an arbitrary angle-of-attack distribution over plan forms whose edges are all supersonic.

In order to obtain the loading over the portions of the panel near the tip, an additional term is needed which will be expressed as a correction to the load coefficient previously obtained for the inboard section of the panel. The method of Evvard (ref. 14) was used in which the effect of the subsonic edge is obtained by a cancellation of a portion of the integration over the wing surface in the equation for the velocity potential. The dimensionless load coefficient $G(x,y)$, which is proportional to the loading from the leading edge to the point x,y, is defined in terms of the velocity potential and circulation function as follows:

$$G = \frac{\Gamma}{Uc_{av}} = \frac{2\varphi}{Uc_{av}} \tag{A8}$$

For regions where no interactions exist between the Mach line reflected from the tip and the inboard end of the panels (regions IV and V in fig. 1), the area of integration is shown in the following sketch.

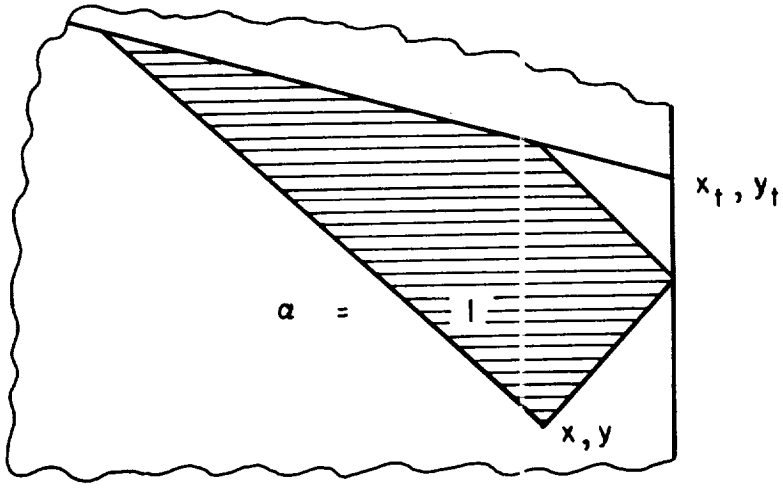

The loss in load coefficient due to the tip was expressed by evaluating the load coefficient obtained from integrating over the shaded area shown in the sketch and subtracting from it a value obtained for the panel without the free edge.

$$G = 0 \qquad (\tau_t < -1) \tag{A9}$$

$$G = \frac{2(x - x_1)}{\pi\beta c_{av}\sqrt{\beta^2 m^2 - 1}} \left\{ -(\beta m - \tau_t)\cos^{-1}\left[\frac{\beta m + \tau_t(2\beta m + 1)}{\tau_t - \beta m}\right] + 2\sqrt{\beta m(-\tau_t)(1 + \tau_t)(\beta m + 1)} \right\} \qquad (-1 \le \tau_t \le 0) \tag{A10}$$

where $0 \le \cos^{-1}(\ ) \le \pi$.

An additional modification of the tip effect must be made for cases where the inboard edge of the panel is relatively close to the tip so that the reflected Mach line from the tip intersects the inboard edge. This condition is given by the equation

$$x - x_1 > \beta(2y_t - y_1 - y) \tag{A11}$$

The region of integration is shown in the following sketch. An examination of the sketch shows that the values of load coefficient for a

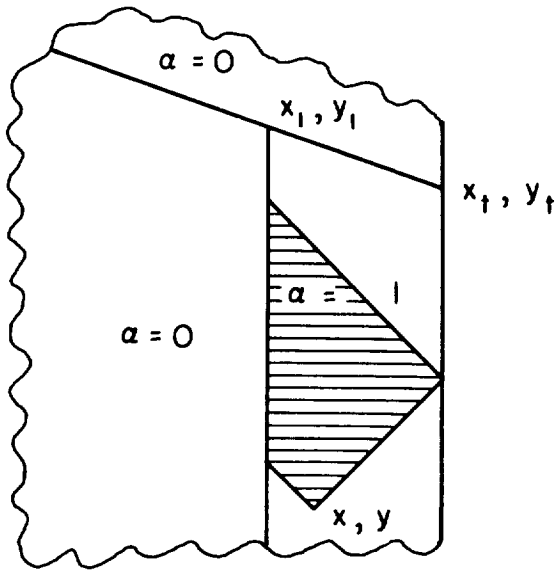

point x,y in region VI of figure 1 are the same as the load coefficient at the boundary between regions V and VI for the same value of y. The load coefficient from the leading edge to a point in region VI can be obtained by substituting the value of the boundary

$$x - x_1 = \beta(2y_t - y_1 - y)$$

into equations (A6) and (A10). These equations can then be combined to give

$$G = \frac{2(y_t - y_1)}{\pi c_{av}} \left[\left(\frac{y - y_1}{y_t - y_1} \right) \cosh^{-1} \left| \frac{2(y_t - y_1)}{y - y_1} - 1 \right| + 2\sqrt{1 - \frac{y - y_1}{y_t - y_1}} \right] \quad (A12)$$

Note that this equation is independent of the leading-edge sweep angle as may be seen from the area of integration shown in the previous sketch.

The equations for the various regions shown in figure 1 are summarized in the main body of the report.

For cases with very low aspect ratios and leading edges just slightly supersonic, another equation must be developed for points on the opposite side of the wing panel from the deflected panel which are affected by the panel and which are defined by the equation

$$x - x_1 > \beta(2y_t + y_1 + y) \quad (A13)$$

The area of integration is indicated by the shaded region in the following sketch.

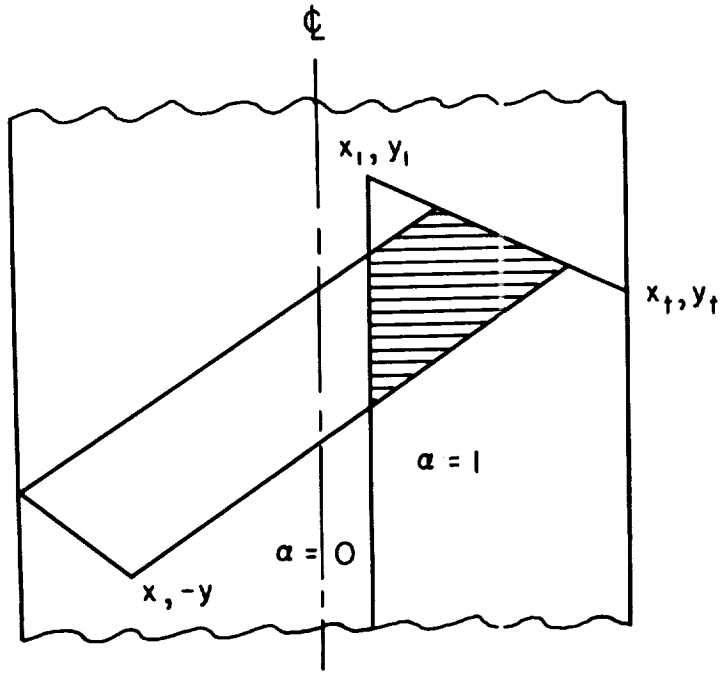

The load coefficient obtained for this region is

$$G = \frac{2}{\pi c_{av}}\left(\left(\frac{mx + y}{\sqrt{\beta^2 m^2 - 1}}\right)\left\{\cos^{-1}\left[\frac{mx - y + 2\beta m(y - y_t) + 2y_t}{mx + y}\right]\right\} + 2\left\{\frac{(y_t - y)[mx + \beta m(y + y_1 - 2y_t) + y_1]}{\beta m + 1}\right\}^{1/2} - (y - y_1)\cosh^{-1}\left|\frac{2(y_t - y_1)}{y_t - y_1} - 1\right|\right) \tag{A14}$$

Fortunately, for most cases, including the lowest Mach number case considered for the example used in this report, the effect of the opposite wing tip from the deflected panel is small, and the load coefficient for this region may be obtained by using equation (A6). This approximation results in including the effect of the extra triangular area near the apex of the panel shown in the previous sketch.

APPENDIX B

DIFFERENTIATING AND INTEGRATING FACTORS USED FOR NUMERICAL EXAMPLE

Two sets of numerical coefficients will be evaluated for the determination of the loading over the flexible wing: (1) the differentiating matrix [D] for differentiating the angle of attack (eq. (11)), and (2) the spanwise integrating matrix [I] for integrating the loading coefficients (eqs. (13), (14), and (21)).

Differentiating Matrix [D]

This portion of the appendix will be concerned with the method used to convert the panel incremental load coefficients to aerodynamic influence coefficients (eq. (11)), that is, coefficients of the form of the incremental load coefficient at one station due to a unit angle of attack at another station, the angle of attack of all other stations being zero. This will make the aerodynamic coefficients compatible with the structural influence coefficients which are expressed as an angle-of-attack distribution. The angle of attack at one station will be defined in terms of the slopes of the neighboring points in both the chordwise and spanwise directions from which the resulting loading may be obtained by use of panel angle-of-attack coefficients. Polynomial curve-fitting methods were used to obtain the slopes (ref. 12), with the degree of the polynomial depending on the accuracy desired.

For the example case, the angle-of-attack variations in the chordwise direction were much less than those in the spanwise direction so that simpler coefficients were used to express the variations in the chordwise direction. The chordwise variations will be considered first. Three equally spaced intervals were used for the exposed portion of the wing panels (fig. 2). Since the [ΔG] coefficients represent loadings due to a panel at a unit angle of attack extending rearward, the arbitrary angle-of-attack distribution is first converted to an incremental angle-of-attack form starting from the leading edge (i.e., coefficients consisting of the slopes at each interval times the interval are formed). For this case the increments can be expressed simply as

$$\Delta\xi \frac{d\alpha}{d\xi} = \Delta\alpha$$

Denoting the leading edge of front, mid, and rear intervals by the subscripts f, m, and r, respectively, the incremental angles of attack may

be written as

$$\left.\begin{aligned} \Delta\alpha_f &= \alpha_f \\ \Delta\alpha_m &= -\alpha_f + \alpha_m \\ \Delta\alpha_r &= -\alpha_m + \alpha_r \end{aligned}\right\} \tag{B1}$$

The left-hand side of equations (B1) denotes a chordwise row location in table III, while the right-hand side indicates a chordwise column location and gives the multiplying factor to be combined with the appropriate spanwise coefficient which will now be evaluated.

For the spanwise variation, the eight control stations used for the angle-of-attack and slope locations are given in the following table.

Station	0	1	2	3	4	5	6	7
α at η	0	0.143	0.286	0.429	0.572	0.715	0.858	1.000
$d\alpha/d\eta$ at η	0	.143	.286	.429	.572	.715	.858	.929

The outboard station for the slope was chosen at a half interval from the tip since the value at the tip would have no effect on the aerodynamic load. The first three angle-of-attack stations denote the portion of the wing blanketed by the fuselage and are used only for angle-of-attack distributions for the rigid case. Hence, the values given in table III apply only for cases where no chordwise variation in angle of attack occurs for these three stations. The slope at each station was obtained by passing a parabola through three adjacent spanwise stations and differentiating the result. The resulting coefficients consisted of the slope times the appropriate interval $[\Delta\eta(d\alpha/d\eta)]$, and are listed as follows:

$$\left.\begin{aligned} \left(\Delta\eta\,\frac{d\alpha}{d\eta}\right)_0 &= \frac{1}{2}\left(-\frac{3}{2}\,\alpha_0 + 2\alpha_1 - \frac{\alpha_2}{2}\right) \\ \left(\Delta\eta\,\frac{d\alpha}{d\eta}\right)_1 &= -\frac{\alpha_0}{2} + \frac{\alpha_2}{2} \\ \left(\Delta\eta\,\frac{d\alpha}{d\eta}\right)_2 &= -\frac{\alpha_1}{2} + \frac{\alpha_3}{2} \\ &\cdots\cdots\cdots\cdots\cdots \\ \left(\Delta\eta\,\frac{d\alpha}{d\eta}\right)_6 &= \frac{3}{4}\left(-\frac{\alpha_5}{2} + \frac{\alpha_7}{2}\right) \\ \left(\Delta\eta\,\frac{d\alpha}{d\eta}\right)_7 &= \frac{1}{2}\left(-\alpha_6 + \alpha_7\right) \end{aligned}\right\} \tag{B2}$$

The left-hand side of equations (B2) indicates a spanwise row location in table III, while the right-hand side denotes a spanwise column location and the corresponding spanwise coefficient to be multiplied with a chordwise coefficient given by equations (B1).

Integrating Matrix [I]

The matrix [I] represents a spanwise integrating matrix for summing the load coefficients (eqs. (13), (14), and (21)). Simpson's rule factors (e.g., ref. 12) which are based on passing a parabola through three adjacent points, were used to integrate over the interval from $\eta = 0$ to $\eta = 0.858$. In order to better approximate the shape of the loading over the interval from $\eta = 0.858$ to the tip, an equation of the following form was used to obtain the integrating factors.

$$G(\eta) = k_0(1 - \eta)^{1/2} + k_1(1 - \eta)^{3/2}$$

The constants k_0 and k_1 were evaluated in terms of the value of $G(\eta)$ at $\eta = 0.858$ and 0.929. The integration constants were then determined from the above equation. The integration constants for the entire span, including the appropriate interval, are given in table IV.

REFERENCES

1. Cole, Henry A., Jr., Brown, Stuart C., and Holleman, Euclid C.: Experimental and Predicted Longitudinal and Lateral-Directional Response Characteristics of a Large Flexible 35° Swept-Wing Airplane at an Altitude of 35,000 Feet. NACA Rep. 1330, 1957.

2. Biot, M. A.: The Divergence of Supersonic Wings Including Chordwise Bending. Jour. Aero. Sci., vol. 23, no. 3, March 1956, pp. 237-251, 271. (Also available as Cornell Aero. Lab., Inc. Rep. CAL-67, Dec. 1954, and IAS Preprint No. 502, 1955)

3. Hedgepeth, John M., and Waner, Paul G., Jr.: Analysis of Static Aeroelastic Behavior of Low-Aspect-Ratio Rectangular Wings. NACA TN 3958, 1957.

4. Pines, Samuel, Dugundji, John, and Neuringer, Joseph: Aerodynamic Flutter Derivatives for a Flexible Wing with Supersonic and Subsonic Edges. Jour. Aero. Sci., vol. 22, no. 10, Oct. 1955, pp. 693-700.

5. Voss, Herbert M., Zartarian, Garabed, and Hsu, Pao-Tan: Application of Numerical Integration Techniques to the Low-Aspect-Ratio Flutter Problem in Subsonic and Supersonic Flows. M.I.T. Aeroelastic and Structures Res. Lab. Rep. 52-3, Contract No. a(s) 53-564-c, Oct. 1954.

6. Stein, Manuel, and Sanders, J. Lyell, Jr.: A Method for Deflection Analysis of Thin Low-Aspect-Ratio Wings. NACA TN 3640, 1956.

7. Turner, M. J., Clough, R. W., Martin, H. C., and Topp, L. J.: Stiffness and Deflection Analysis of Complex Structures. Jour. Aero. Sci., vol. 23, no. 9, Sept. 1956, pp. 805-823, 854.

8. Schuerch, Hans U.: Structural Analysis of Swept, Low Aspect Ratio, Multispar Aircraft Wings. Aero. Eng. Review, vol. 11, no. 11, Nov. 1952, pp. 34-41. (Also available as IAS Preprint No. 377, 1952, and Convair Rep. ZS-147A, Sept. 1952)

9. Williams, D.: Recent Developments in the Structural Approach to Aeroelastic Problems. Royal Aero. Soc., vol. 58, no. 522, June 1954, pp. 403-428.

10. Levy, Samuel: Structural Analysis and Influence Coefficients for Delta Wings. Jour. Aero. Sci., vol. 20, no. 7, July 1953, pp. 449-454. (Also available as Nat. Bur. of Standards Rep. 2031, Oct. 1952)

11. Skoog, Richard B., and Brown, Harvey H.: A Method for the Determination of the Spanwise Load Distribution of a Flexible Swept Wing at Subsonic Speeds. NACA TN 2222, 1951. (Supersedes NACA RM A50G31)

12. Milne, William Edmund: Numerical Calculus. Princeton University Press, Princeton, N. J., 1949.

13. Lagerstrom, P. A., and Graham, Martha E.: Linearized Theory of Supersonic Control Surfaces. Jour. Aero. Sci., vol. 16, no. 1, Jan. 1949, pp. 31-34. (Also available as Rep. SM-13060, Douglas Aircraft Co., Inc., July 1947, and IAS Preprint No. 131, 1948)

14. Evvard, John C.: Use of Source Distributions for Evaluating Theoretical Aerodynamics of Thin Finite Wings at Supersonic Speeds. NACA Rep. 951, 1950.

TABLE I.- STRUCTURAL INFLUENCE COEFFICIENTS

Streamwise angular deflection times $E(t/c)^3 S_p$ at station, radians		Upload at station, lb														
	η	0.429			0.572			0.715			0.858			0.929		
		f	m	r	f	m	r	f	m	r	f	m	r	f	m	r
0.429	f	6.2	0.8	-2.0	4.2	-1.9	-1.5	3.7	-3.6	-2.1	3.2	-8.3	-2.6	3.5	-5.3	-5.4
	m	4.6	.8	-4.4	3.0	-.3	-5.7	2.4	-2.8	-7.4	.7	-7.7	-9.2	.7	-5.0	-10.9
	r	2.8	1.0	-8.1	1.7	.5	-13.0	1.4	-1.3	-18.0	1.8	-7.7	-22.1	2.2	-5.0	-24.2
0.572	f	5.2	.2	-5.8	5.9	-2.0	-9.1	8.6	-7.8	-13.9	9.9	-16.5	-18.2	9.8	-17.6	-21.6
	m	3.6	.9	-9.3	4.9	-1.3	-17.3	7.6	-6.9	-23.9	7.9	-15.1	-29.3	5.8	-16.5	-30.9
	r	2.4	.7	-12.0	4.5	0	-26.9	6.1	-4.0	-43.1	5.0	-12.8	-55.3	4.7	-15.8	-58.2
0.715	f	3.8	-.1	-8.7	7.2	-2.6	-18.3	12.1	-12.4	-30.1	16.1	-26.0	-38.6	16.0	-30.4	-45.5
	m	2.5	1.1	-13.8	5.9	-2.3	-29.1	9.8	-10.5	-44.7	12.3	-24.7	-59.0	13.5	-29.6	-67.7
	r	1.6	.1	-16.7	5.4	-.7	-39.6	8.6	-7.4	-69.2	13.9	-19.9	-103.4	12.0	-26.9	-94.6
0.858	f	2.4	.4	-14.4	6.0	-3.0	-28.1	14.3	-15.1	-49.6	21.6	-32.4	-70.4	22.4	-47.1	-83.7
	m	1.0	.6	-17.6	4.9	-2.7	-36.5	12.6	-13.1	-67.8	20.6	-30.5	-91.0	20.4	-45.4	-107.5
	r	.9	.2	-19.6	4.1	-1.7	-42.3	9.8	-11.6	-76.6	18.3	-26.6	-114.9	18.2	-42.2	-131.3
1.000	f	2.7	-.9	-18.5	4.5	-2.8	-36.2	12.9	-17.3	-65.8	23.9	-38.0	-104.5	26.7	-60.6	-132.6
	m	2.3	-.8	-20.6	4.2	-2.6	-39.8	11.5	-15.9	-72.0	23.4	-35.0	-115.8	25.7	-58.7	-146.3
	r	2.2	-.8	-20.6	3.7	-2.5	-41.4	10.8	-15.5	-76.7	22.0	-34.1	-119.5	24.4	-56.9	-153.4

Note: The front, mid, and rear locations shown in figure 2 are denoted by f, m, and r.

TABLE II.- MATRIX [B]

η		0	0.143	0.286	0.429			0.572			0.715			0.858			0.929		
					f	m	r	f	m	r	f	m	r	f	m	r	f	m	r
0		1																	
0.143			1																
0.286				1															
0.429	f				1														
	m				-1	1													
	r					-1	1												
0.572	f							1											
	m							-1	1										
	r								-1	1									
0.715	f										1								
	m										-1	1							
	r											-1	1						
0.858	f													1					
	m													-1	1				
	r														-1	1			
0.929	f																1		
	m																-1	1	
	r																	-1	1

TABLE III.- DIFFERENTIATING MATRIX [D]

η		0	0.143	0.286	0.429			0.572			0.715			0.858			1.000		
					f	m	r	f	m	r	f	m	r	f	m	r	f	m	r
0		-3/4	1	-1/4															
0.143		-1/2		1/2															
0.286	f		-1/2		1/2														
	m				-1/2	1/2													
	r					-1/2	1/2												
0.429	f			-1/2				1/2											
	m							-1/2	1/2										
	r								-1/2	1/2									
0.572	f				-1/2						1/2								
	m				1/2	-1/2					-1/2	1/2							
	r					1/2	-1/2					-1/2	1/2						
0.715	f							-1/2						1/2					
	m							1/2	-1/2					-1/2	1/2				
	r								1/2	-1/2					-1/2	1/2			
0.858	f										-3/8						3/8		
	m										3/8	-3/8					-3/8	3/8	
	r											3/8	-3/8					-3/8	3/8
0.929	f													-1/2			1/2		
	m													1/2	-1/2		-1/2	1/2	
	r														1/2	-1/2		-1/2	1/2

TABLE IV.- INTEGRATING MATRIX [I]

η		0	0.143	0.286	0.429			0.572			0.715			0.858			0.929		
					f	m	r	f	m	r	f	m	r	f	m	r	f	m	r
0		0.0476																	
0.143			0.1905																
0.286				0.0952															
0.429	f				0.1905														
	m					0.1905													
	r						0.1905												
0.572	f							0.0952											
	m								0.0952										
	r									0.0952									
0.715	f										0.1905								
	m											0.1905							
	r												0.1905						
0.858	f													0.0667					
	m														0.0667				
	r															0.0667			
0.929	f																0.1078		
	m																	0.1078	
	r																		0.1078

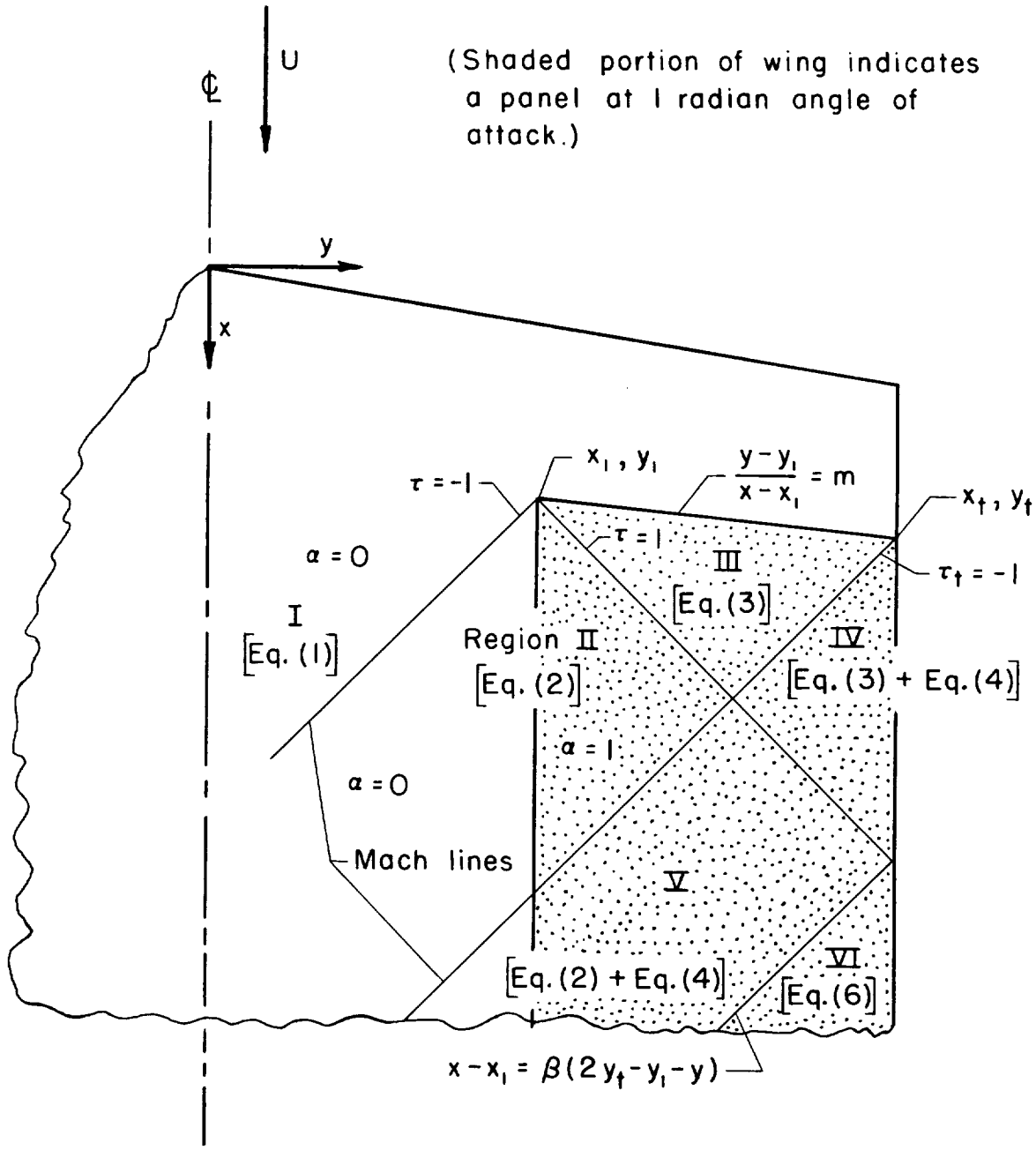

Figure 1.- Coordinate system and regions of influence for panel at angle of attack.

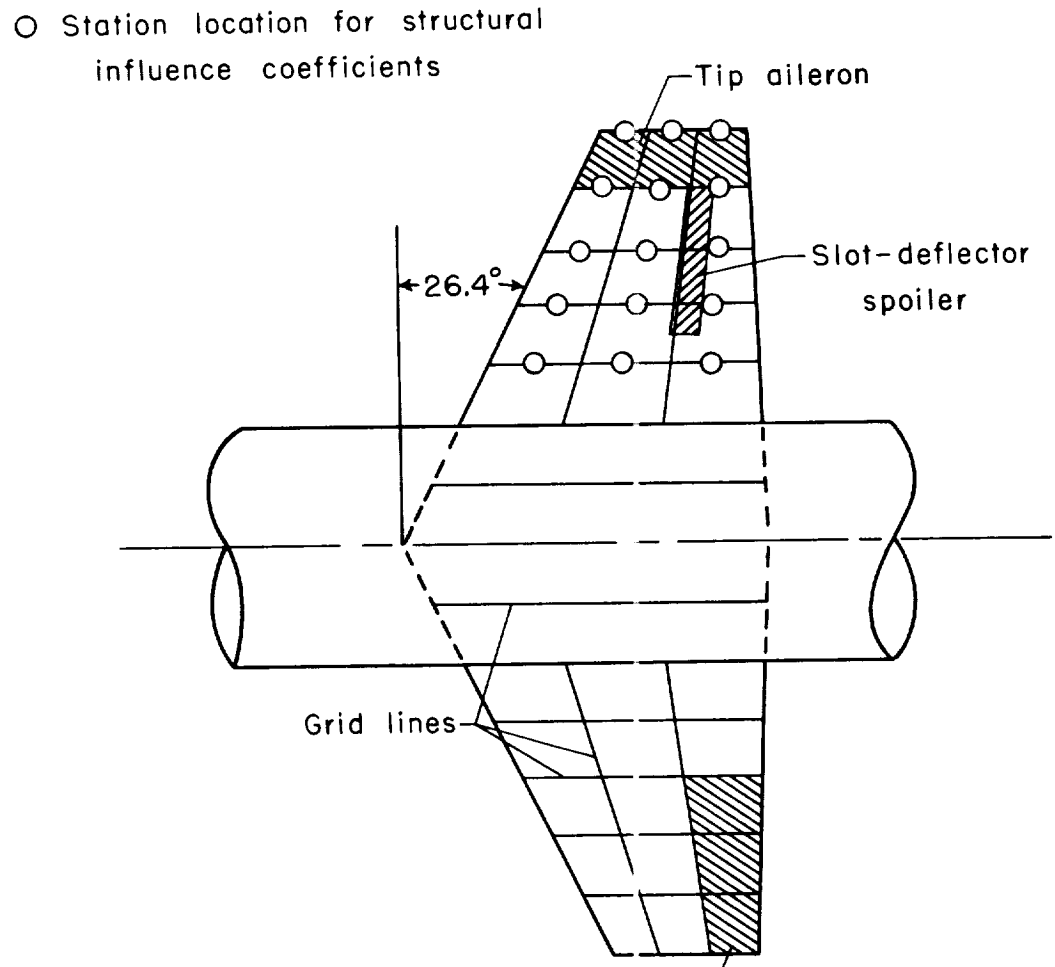

Figure 2.- Geometric characteristics of numerical example.

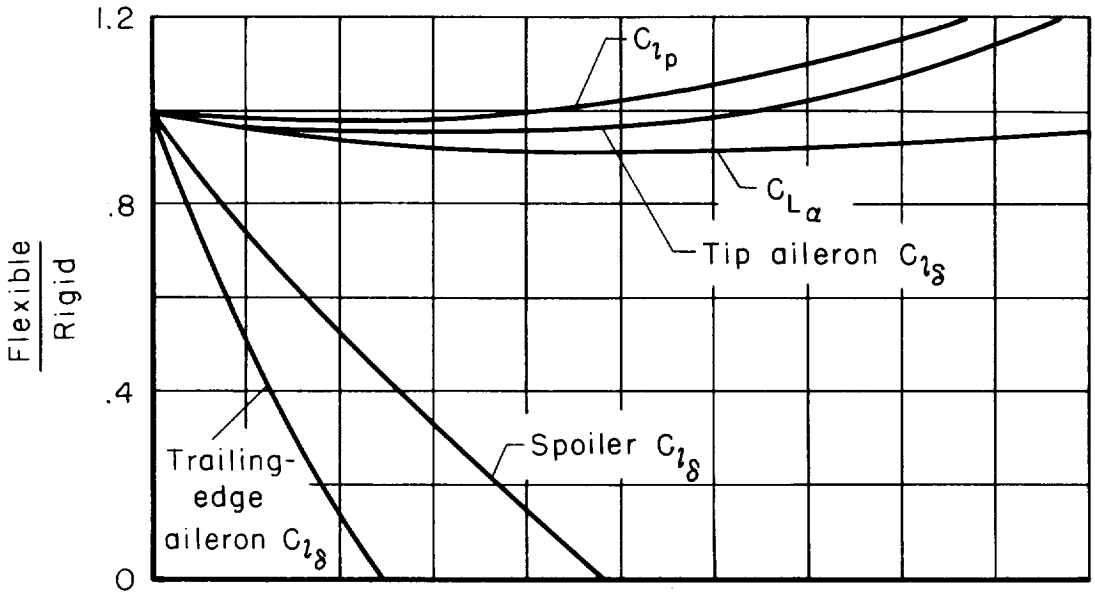

(a) M = 1.25

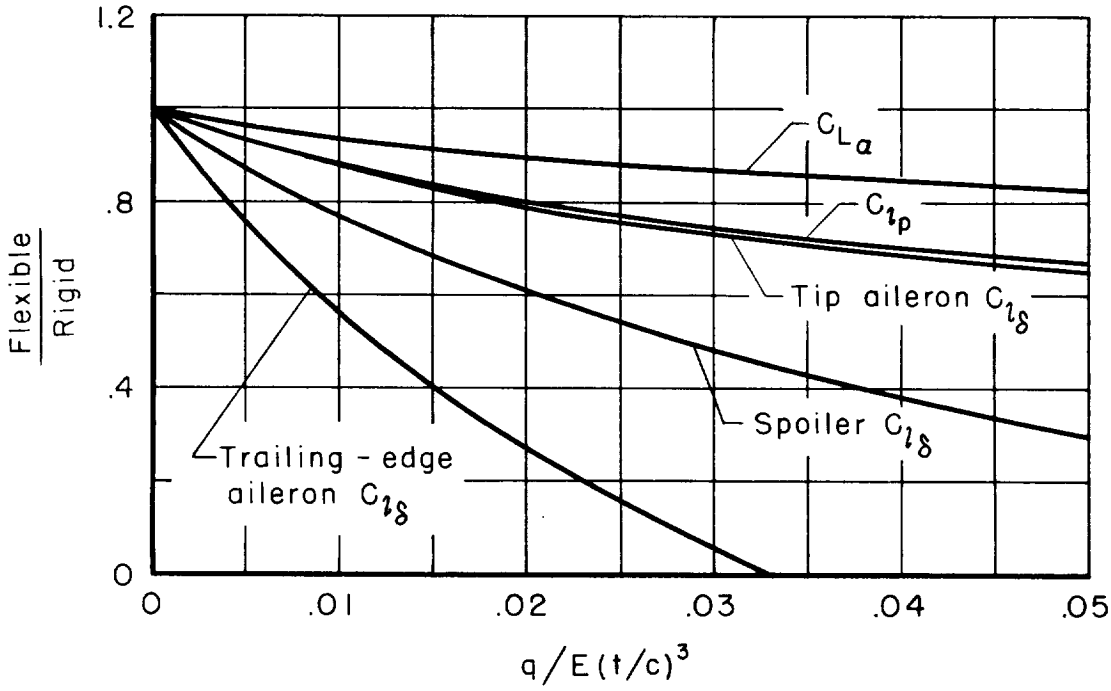

(b) M = 2.60

Figure 3.- Variation of rolling and lift effectiveness with dynamic pressure.

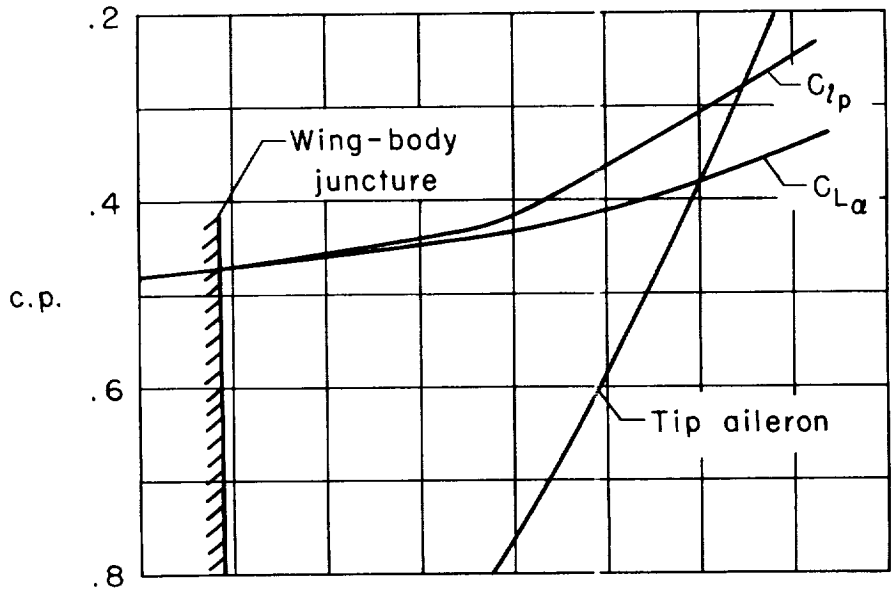

(a) M = 1.25

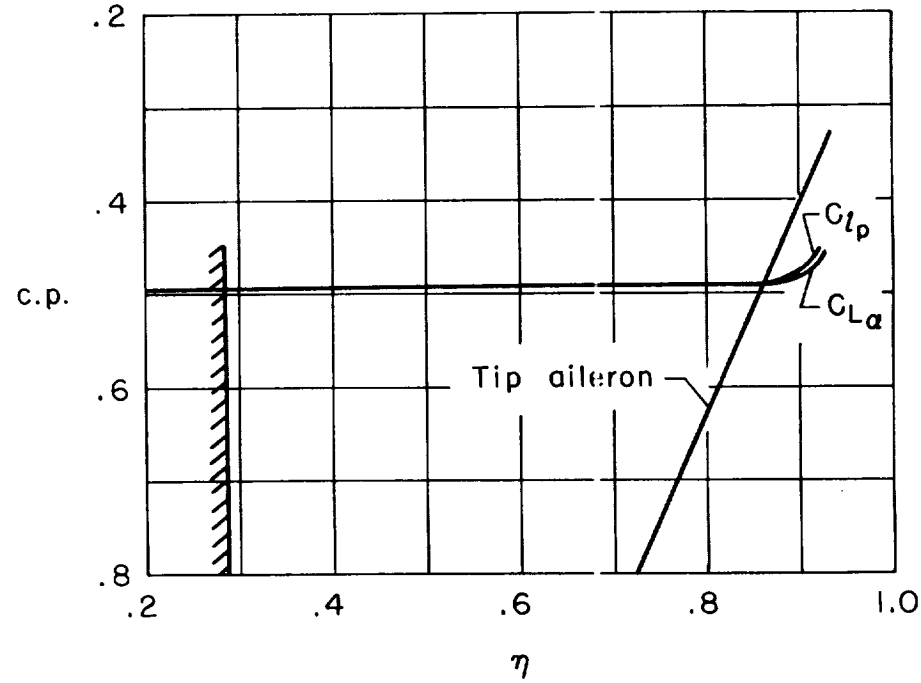

(b) M = 2.50

Figure 4.- Centers of pressure of rigid-wing loadings.

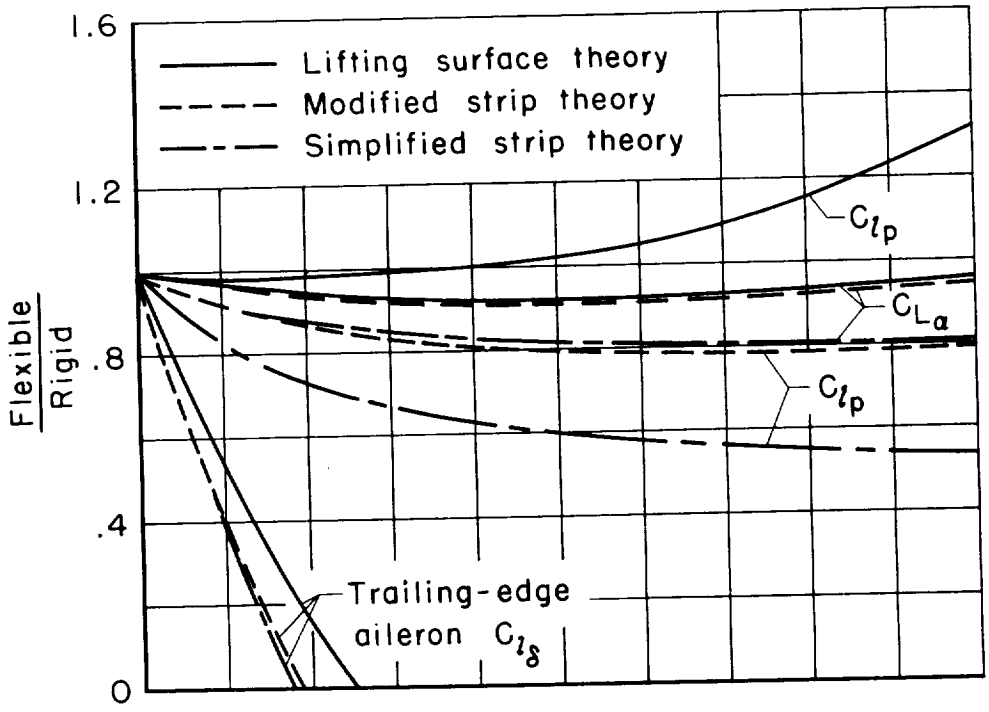

(a) M = 1.25

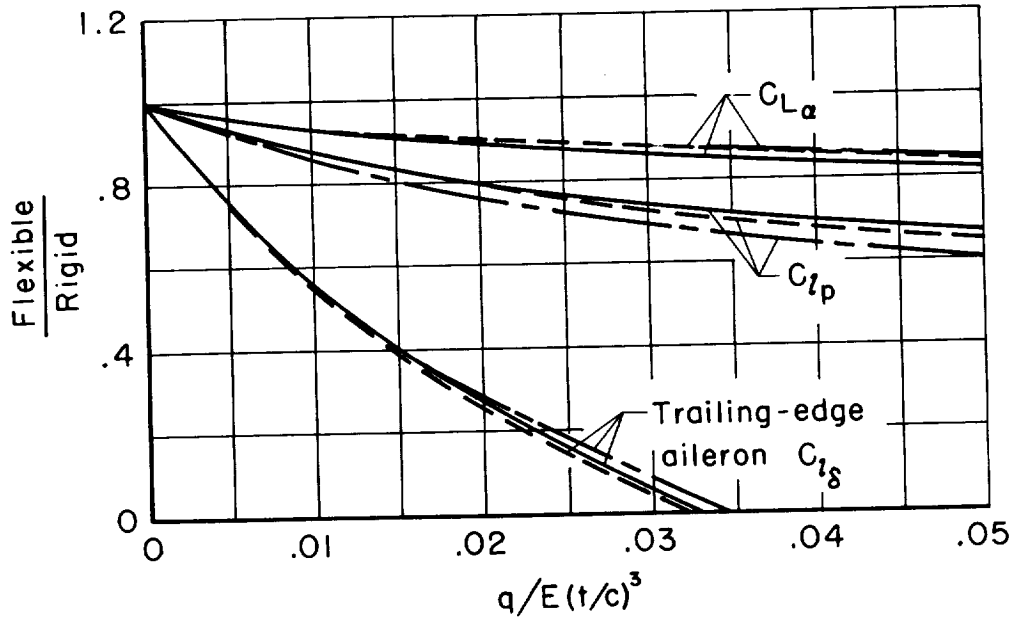

(b) M = 2.60

Figure 5.- Comparisons of lifting surface theory results with strip theory results.

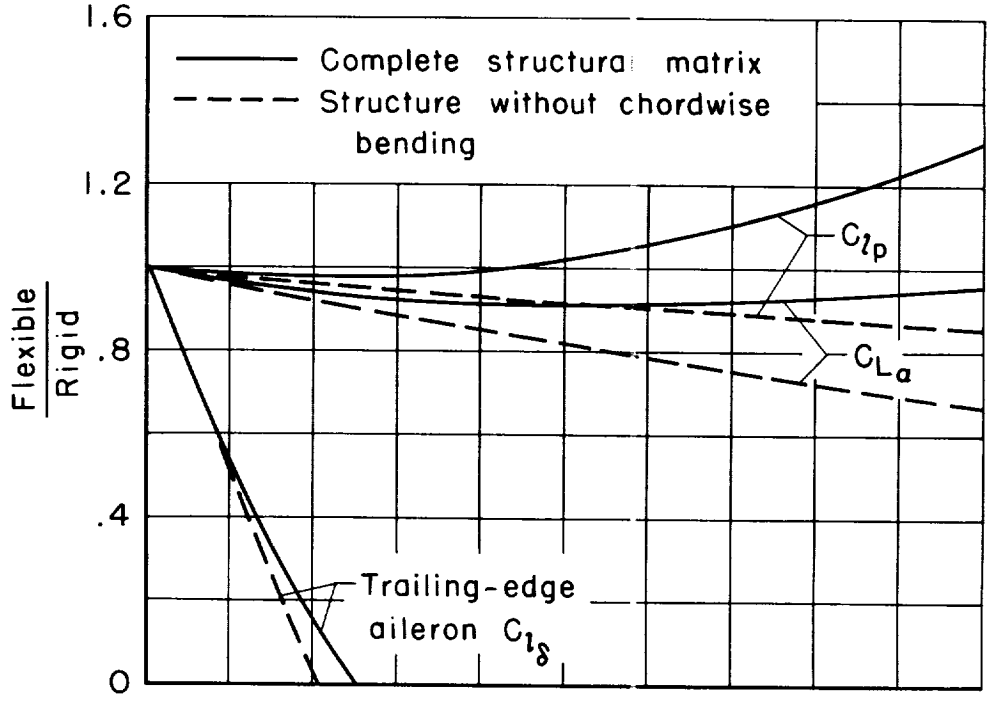

(a) M = 1.25

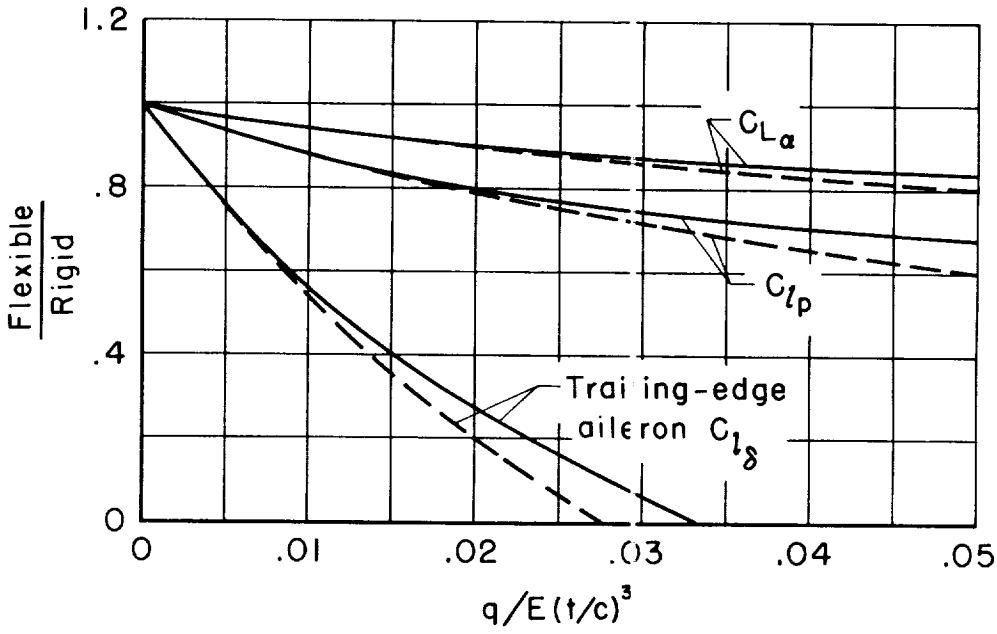

(b) M = 2.60

Figure 6.- Effect of chordwise bending on rolling and lift effectiveness.

NASA - Langley Field, Va. A-159